X-Band Polarimetric Radar Measurements of Rainfall

SERGEY Y. MATROSOV

Cooperative Institute for Research in Environmental Sciences, University of Colorado, and NOAA/Environmental Technology Laboratory, Boulder, Colorado

KURT A. CLARK AND BROOKS E. MARTNER

NOAA/Environmental Technology Laboratory, Boulder, Colorado

ALI TOKAY

Joint Center for Earth Systems Technology, University of Maryland, Baltimore County, Baltimore, Maryland

(Manuscript received 18 December 2001, in final form 13 May 2002)

ABSTRACT

A combined polarimetric estimator for rainfall rate (R) retrievals from polarimetric radar measurements at X band is proposed. This estimator uses the horizontal polarization radar reflectivity Z_e, differential reflectivity Z_{DR}, and specific differential phase shift K_{DP}, and it intrinsically accounts for changes in how drop oblateness increases with size. Because this estimator uses power measurements (i.e., Z_e and Z_{DR}), a procedure for correcting these measurements for effects of partial attenuation and differential attenuation using the differential phase measurement is suggested. An altitude correction for estimates of rainfall rates is also suggested. The proposed combined polarimetric estimator that uses K_{DP}, Z_{DR}, and Z_e, an estimator that uses K_{DP} alone for equilibrium drop shapes, and different Z_e–R relations were applied to the 15 rain events observed with the NOAA X-band transportable polarimetric radar during the eight-week field campaign at the NASA Wallops Island facility in Virginia. The observed rains ranged from very light stratiform events to very heavy convective ones with cells producing rainfall rates in excess of 100 mm h^{-1}. The three different ground validation sites were equipped with high-resolution (0.01 in.) tipping-bucket rain gauges. One of these sites also was equipped with disdrometers. In terms of the relative standard deviation, the combined polarimetric estimator provided the best overall agreement with gauge data (22%), closely followed by a case-tuned Z_e–R relation (23%) that was determined for each observational case from drop size distributions (DSD) measured in situ by a disdrometer and was available only a posteriori. The use of the K_{DP}-only estimator and a mean Z_e–R relation resulted in 30% and 32% relative standard deviations, correspondingly. The combined polarimetric estimator, the K_{DP}-only estimator, and the case-tuned Z_e–R relation estimator provided about a 6%–9% negative bias in comparison with the gauge data; the mean Z_e–R relation estimator provided a larger negative bias (18%).

1. Introduction

Improvement of rainfall parameter estimates from radar measurements has been one of the priorities of radar meteorology. It is generally accepted that the use of radar polarization parameters in the linear polarimetric basis improves quantitative estimates of rainfall rate. The radar polarization parameters of main interest for improving rainfall estimates are the specific differential propagational phase shift K_{DP} and differential reflectivity Z_{DR}.

Most research in the field of radar polarimetry as applied to rainfall parameter estimates has been performed for the radar wavelengths at S band ($\lambda \sim 10$–11 cm; e.g., Zrnić and Ryzhkov 1996; Chandrasekar et al. 1990) and C band ($\lambda \sim 5$–6 cm; e.g., May et al. 1999). These are the wavelengths of operational radars in many countries [e.g., the S-band Weather Surveillance Radar-1988 Doppler (WSR-88D) network in the United States]. Longer radar wavelengths (such as those at S band) are the obvious choice for measurements in moderate and heavy rain because of low attenuation and backscatter phase shifts effects. Partial attenuation of radar signals is already a problem at C-band frequencies. A number of studies have suggested and discussed several polarimetric and nonpolarimetric approaches for correcting partial attenuation at C band (e.g., Gorgucci et al. 1998; Carey et al. 2000).

Many research and some operational meteorological radars employ shorter wavelengths, such as those at X band ($\lambda \sim 3$ cm). The partial attenuation effects at X band are more severe when compared with those at C band, and accounting for these effects has been a significant problem for quantitative estimates of rainfall parameters based on reflectivity measurements at these

Corresponding author address: Dr. Sergey Y. Matrosov, CIRES, University of Colorado, and NOAA/Environmental Technology Laboratory, 325 Broadway, R/ET7, Boulder, CO 80305.
E-mail: sergey.matrosov@noaa.gov

wavelengths. Introducing polarimetric diversity (viz., a differential phase shift capability) for X-band radars allows a robust way to account for attenuation effects, thus overcoming this drawback of X-band wavelengths in many situations. Moreover, the total attenuation constraint can be used for rain profiling similar to the spaceborne radar algorithms (e.g., Testud et al. 2000).

The use of shorter wavelengths, such as those at X band, has certain advantages over use of longer wavelengths with regard to polarimetric measurements in light and moderate rains (Matrosov et al. 1999). This includes a stronger, more readily detectable propagation differential phase shift that is proportional to the reciprocal of the wavelength for the Rayleigh conditions. At X band this amounts to about a factor-of-3 increase when compared with S band (a factor of about 1.7 in comparison with C band). Scattering and extinction of X-band wavelengths in rain has still largely the Rayleigh-type behavior except for possible backscatter phase shifts for larger rain drops.

X-band radars have additional advantages that make them a convenient tool and an appropriate choice for some practical applications. For a given transmitter power and antenna size, shorter wavelengths offer greatly increased sensitivity for detecting weak targets. As a result, these radars are generally relatively small and inexpensive and can be more easily transported to new locations than can S-band systems. Most X-band radars offer better spatial resolution and less problematic ground clutter than large S-band radars. As such, they are well suited to uses where transportability and fine-scale observations are important, such as in hydrometeorological studies across moderately sized complex terrain watersheds and urban basins. They may also be useful for filling critical gaps in the coverage of operational radar networks. These advantages and applications will increase since the partial attenuation problem that has limited the use of X band for quantitative rainfall estimations is being alleviated. Longer wavelength radars would still be the prime choice for wide-scale weather surveillance, but X-band systems would be able to contribute in important new ways to research and operations.

Over the last few years, the National Oceanic and Atmospheric Administration's (NOAA) Environmental Technology Laboratory (ETL) has upgraded one of its X-band radars (Martner et al. 2001). This 3.2-cm-wavelength transportable radar (X pol) now is fully polarimetric and has full Doppler and scanning capabilities. Initial X-band differential phase shift measurement tests with the X-pol radar in moderate stratiform rains indicated no significant contributions from the backscatter phase shift (Matrosov et al. 1999). During these tests, K_{DP}-based rainfall rate estimators for X band provided a generally satisfactory agreement between rainfall accumulations derived from the radar data and accumulations measured by high-resolution rain gauges. These estimators are relatively insensitive to the details of drop size distributions (Zrnić and Ryzhkov 1996); however, they depend rather significantly on the model relating raindrop shape and drop size. Variability of this shape–size relation contributes a significant uncertainty of rainfall estimators that are based solely on the differential phase measurements. In this paper, we suggest and evaluate a combined rainfall rate X-band polarimetric estimator that uses measurements of differential phase shift, differential reflectivity, and the horizontal polarization reflectivity. This estimator intrinsically accounts for a changing degree of drop oblateness (i.e., drop shape) as a function of drop size.

2. Modeling of rainfall rate estimators at X band

It has been demonstrated for the S-band frequency radars that the addition of the polarimetric information usually improves accuracy of the rainfall rate R and accumulation A retrievals when compared with traditional approaches based only on measurements of equivalent radar reflectivity Z_e (Ryzhkov and Zrnić 1995). More recent studies (e.g., Brandes et al. 2001) showed, however, that rainfall estimates obtained with a fixed coefficient K_{DP}–R relation are similar to those obtained from the radar reflectivity only given that the radar is well calibrated. These results indicate that simple estimators relying on just one polarization parameter may not provide a sizable improvement over traditional approaches, and that combined polarimetric estimators may be needed.

a. K_{DP}–R relations at X band

Most theoretical studies of K_{DP}–R relations were performed assuming the equilibrium drop shape model, which predicts an almost linear decrease of the spheroidal raindrop aspect ratio r as a function of D_e: $r = 1.03 - 0.62D_e$. This equation gives aspect ratios close to those in data of Pruppacher and Pitter (1971). Drops less than about 0.05 cm were usually assumed to be spherical in shape.

A number of recent studies (e.g., Kubesh and Beard 1993; Keenan et al. 1997; Andsager et al. 1999; Gorgucci et al. 2000, 2001) indicate that the equilibrium drop shape is not unique and the variability in drop aspect ratio–diameter relations can be significant. Assuming a mostly linear trend of aspect ratio decrease with size, the following generalized r–D_e relation can be suggested:

$$r = (1.0 + 0.05b) - bD_e \qquad (D_e > 0.05 \text{ cm}), \quad (1)$$

where b is the shape factor in inverse centimeters. Note that aspect ratio model (1) differs from the one suggested earlier by Gorgucci et al. (2000) by assuming that for all values of b, drops smaller than 0.05 cm are spherical. This assumption is substantiated by various microphysical studies (e.g., Pruppacher and Klett 1978).

Figure 1 shows the results of modeling K_{DP}–R relations for a radar wavelength of 3.2 cm for eight different values

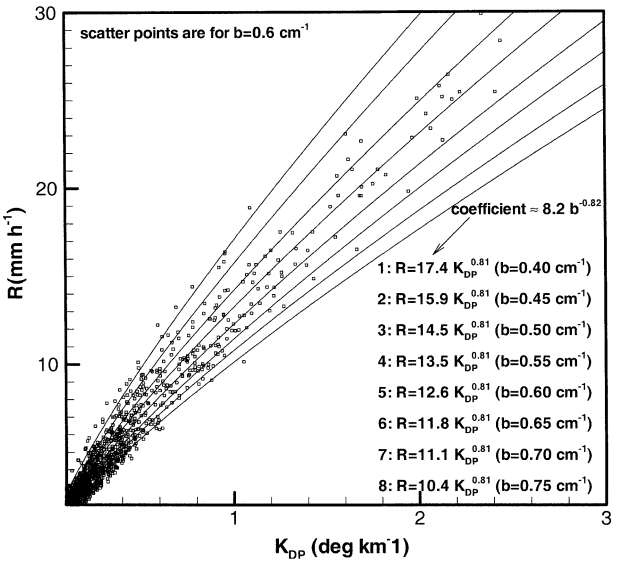

FIG. 1. X-band K_{DP}–R relations for different values of the shape factor b.

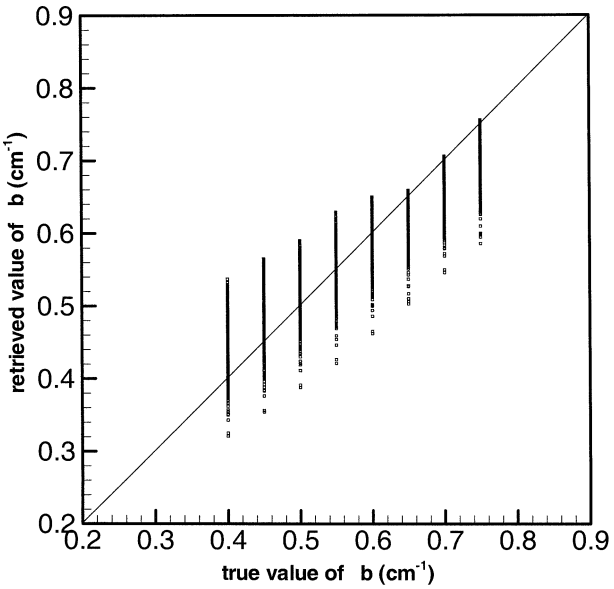

FIG. 2. Scatterplot between true values of the shape factor b and its estimates from Eq. (3).

of the shape factor b in the range from 0.4 to 0.8 cm^{-1}, which covers most of the dynamic range of natural changes of this parameter according to the case study of Gorgucci et al. (2000). The T-matrix approach for spheroidal shape drops was used for calculations (Barber and Yeh 1975). In order not to clutter the graph, the individual modeling results in Fig. 1 are depicted for $b = 0.6$ cm^{-1}, which approximately corresponds to the equilibrium drop shape while the power-law best-fit regressions are drawn for all considered values of b. The corresponding regressions are also shown in Fig. 1.

Experimental size spectra rather than model drop size distributions (DSD) were used to derive K_{DP}–R relations in Fig. 1. These DSD spectra were 1-min averages recorded using an impact Joss–Waldvogel disdrometer during the two-month-long field observation campaign held at Wallops Island, Virginia, from 21 February to 19 April 2001. The observed rainfalls ranged from very light (about 1 mm h^{-1}) to very heavy rain (exceeding, at times, 100 mm h^{-1}). Both stratiform and convective rain types are present in the DSD dataset. The total number of DSD spectra used for modeling was about 3450. All measured DSD spectra were quality controlled. For most of the events considered here, the total rainfall accumulations estimated from disdrometer data usually were within 10% of measurements of collocated high-resolution (0.01 in.) tipping-bucket-type rain gauges.

As can be seen from modeling results in Fig. 1, the value of the exponent in K_{DP}–R relations is fairly independent of the assumption about the shape factor b. The coefficient in these relations, however, depends on b very strongly. A relation between rainfall rate and specific differential phase shift for changing value of b can be expressed as

$$R\ (\text{mm h}^{-1}) \approx 8.2 b^{-0.82} K_{DP}^{0.81}\ (^\circ\ \text{km}^{-1}) \quad (b\text{: cm}^{-1}). \tag{2}$$

The natural variability of the shape factor b contributes significantly to the uncertainty of K_{DP}–R relations since the rainfall estimate almost inversely depends on b. Another source of the uncertainty in K_{DP}–R relations is the variability in the DSD details (Keenan et al. 2001; Zrnić et al. 2000), although the influence of DSD is much smaller here in comparison with that for reflectivity–rain rate relations. For the Wallops experiment DSDs, the uncertainty in K_{DP}–R relations due to DSD details (expressed in terms of the relative standard deviation of individual data points when a value of b is fixed) is about 15%. It can be seen from equations in Fig. 1 that the similar uncertainty is caused by about 0.08–0.1 cm^{-1} variability in b.

Gorgucci et al. (2001) showed that the shape factor b can be estimated from combined measurements of the horizontal polarization reflectivity Z_{eh}, Z_{DR}, and K_{DP}. Applying their approach suggested for S band to X band yields the following multidimensional nonlinear regression:

$$b\ (\text{cm}^{-1}) \approx 12 Z_{eh}^{-0.36}\ (\text{mm}^6\ \text{m}^{-3}) K_{DP}^{0.40}\ (^\circ\ \text{km}^{-1}) Z_{dr}^{1.02}. \tag{3}$$

In (3) Z_{dr} is expressed in linear units as opposed to the traditional definition of Z_{DR} in decibels ($Z_{DR} = 10 \log_{10} Z_{dr}$). This distinction is denoted by the use of lowercase letters in the subscript rather than uppercase ones (Z_{dr} vs Z_{DR}).

Figure 2 shows the scatterplot between the estimated value of the shape factor b_e, which was calculated using (3), and the true value of b used for modeling of Z_{eh}, K_{DP},

and Z_{dr}. The calculations were performed for all the 3450 DSDs from the Wallops experiment using values of b from 0.4 to 0.75 cm^{-1} with an increment of 0.05 cm^{-1}. The regression (3) provides no overall bias, though it is biased negatively for larger values of b and positively for smaller values of b. The overall relative standard deviation is about 8%, which is a quantitative measure of quality of shape factor estimations using the regression (3). The 8% error in b estimates is probably acceptable for practical reasons since it introduces less uncertainty in K_{DP}–R relations than the effects of DSD details.

b. X-band combined polarimetric estimator of rainfall rate

Substituting estimates of the shape factor b from (3) in (2) results in a rainfall rate estimator that uses three radar parameters:

$$R \approx c(h)1.06Z_{eh}^{0.3}K_{DP}^{0.50}Z_{dr}^{-0.84}, \quad (4)$$

where c is the altitude correction coefficient. This coefficient accounts for the drop fall velocity changes with altitude h above sea level caused by change in the density of ambient air. It is usually ignored, though it may contribute to noticeable differences when comparing the results of radar measurements from near–sea level sites and ones that are relatively high above sea level. Since the drop terminal velocities are inversely proportional approximately to the 0.45th power of the air density ρ (Beard 1985), the altitude correction coefficient $c(h)$ can be expressed as

$$c(h) \approx 1.1\rho(h)^{-0.45}, \quad (5)$$

where the air density is in kilograms per cubic meter.

Though the combined X-band polarimetric estimator for instantaneous rainfall rates (4) was obtained using the experimental DSDs from a two-month-long period of rains on the Virginia coast, it might work for other geographical locations as well. This is supported by the fact that a procedure similar to the procedure described above for obtaining Z_{eh}–K_{DP}–Z_{dr} estimators based on 140 DSD disdrometer measurements from the Tropical Rainfall Measuring Mission Texas and Florida Underflights Phase A experiment near Houston, Texas, leads to a regression (Matrosov et al. 2001) that provides rainfall rates that are very close (within 10% typically) to those obtained using (4) for the most common rain reflectivity range 30–50 dBZ.

One of the reasons for this relative stability is the comparatively low sensitivity of (2) to the details of DSD (for a given value of b). Another factor contributing to it is the relatively low variability of the shape factor estimator (3) due to DSD changes. This estimator, obtained here for X band, is very close to the S-band relation suggested by Gorgucci et al. (2000) after the K_{DP} wavelength dependence is accounted for. This fact is quite remarkable since results of this paper are based on experimental DSDs, while Gorgucci et al. (2000) used modeled drop spectra.

c. Accounting for partial attenuation

Attenuation of radar signals has been traditionally a significant limitation in using X-band radars for quantitative measurements of rainfall. The K_{DP}-only-based approaches for retrieving rainfall rates are immune to the partial attenuation of radar signals. The combined polarimetric estimator (4), however, also uses power measurements of Z_{eh} and Z_{dr}, which are subject to attenuation and differential attenuation, correspondingly. Different attenuation correction schemes, which adjust reflectivity measurements at a given range based on rainfall rates retrieved for closer ranges and empirical attenuation–rainfall rate relations, are often unstable, which results in the divergence of reflectivity estimates with range. Fortunately, the differential phase polarimetric capability provides a relatively robust way to overcome the partial attenuation problem.

Specific horizontal polarization attenuation A_h, specific differential attenuation A_{DP}, and specific propagational differential phase K_{DP} are all related since they are obtained by integrating the forward scattering amplitudes on horizontal polarization, f_h, and vertical polarization, f_v. These amplitudes define the propagation parameter

$$K_{h,v} = k_o + (2\pi k_o^{-1}) \int_0^{D_{max}} f_{h,v}(D_e)N(D_e)\, dD_e \quad (D_{max} \approx 6 \text{ mm}), \quad (6)$$

where the integration is carried over the drop size distribution $N(D_e)$ and k_o is the wavenumber.

The specific attenuation and the specific phase rotation are given by

$$A_{h,v} = 2\lambda \int_0^{D_{max}} \text{Im}[f_{h,v}(D_e)]N(D_e)\, dD_e, \quad (7)$$

$$\phi_{h,v} = \lambda \int_0^{D_{max}} \text{Re}[f_{h,v}(D_e)]N(D_e)\, dD_e, \quad (8)$$

where $\phi_{h,v}$ is in radians per unit length and $A_{h,v}$ is in the reciprocal of length. Note that $A_{h,v}$ represents the power attenuation, which explains a factor of 2 in (7). The forward scattering amplitudes relate to the dimensionless amplitude matrix elements used in optics, $S_{h,v}$, (e.g., Bohren and Huffman 1983) as

$$S_{h,v} = -2\pi i f_{h,v}\lambda^{-1}. \quad (9)$$

The specific differential attenuation and differential phase shift on propagation are given by

$$A_{DP} = A_h - A_v, \quad (10)$$

$$K_{DP} = \phi_h - \phi_v. \quad (11)$$

Figure 3 shows the scatterplot between A_h and K_{DP} values calculated using the Wallops dataset of DSDs.

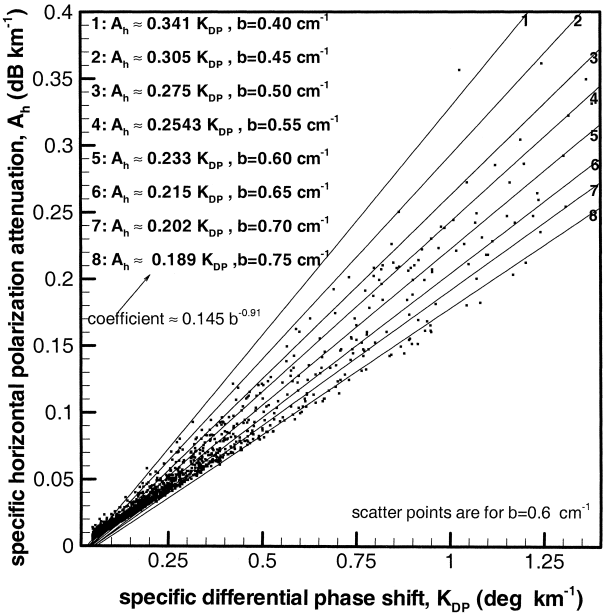

FIG. 3. The A_h–K_{DP} relations for different values of the shape factor b.

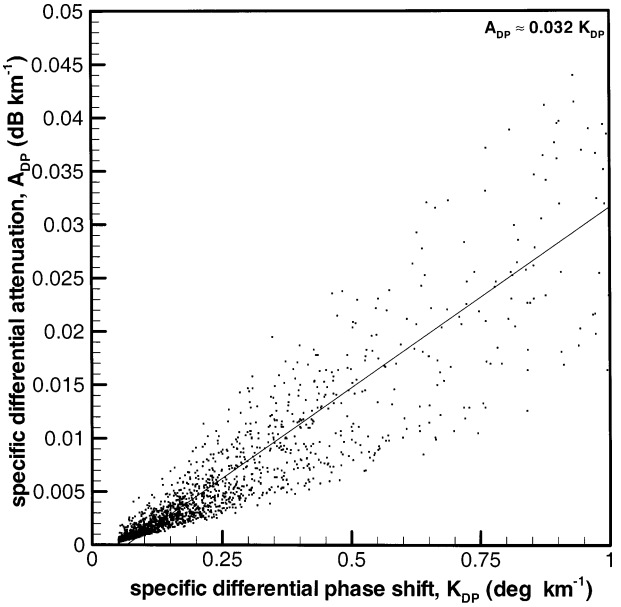

FIG. 4. The A_{DP}–K_{DP} relations.

The assumed temperature is 5°C. The A_h–K_{DP} relations are practically linear. As in Fig. 1, the symbols show results of modeling for the equilibrium drop shape ($b = 0.62$ cm^{-1}), but the best-fit linear regressions are depicted for eight values of b in the range from 0.4 to 0.75 cm^{-1}. For the equilibrium drop shape the coefficient in the $A_h = a_1 K_{DP}$ relation is about 0.22 dB $^{\circ -1}$, which is quite close to the estimate of Bringi et al. (1990), $a_1 = 0.247$ dB $^{\circ -1}$, and Jameson (1991), $a_1 = 0.21$ dB $^{\circ -1}$, which were obtained using the simulated gamma function DSDs. This coefficient exhibits, however, a significant dependence on the shape parameter b, which can be approximated as

$$a_1 \approx 0.145 b^{-0.91}. \tag{12}$$

The total attenuation correction for horizontal polarization reflectivity measurements can be easily estimated from the accumulated propagation differential phase shift Φ_{DP}:

$$\Delta Z_{eh}\ (\mathrm{dB}Z) \approx a_1 \Phi_{DP}\ (^{\circ}). \tag{13}$$

Figure 4 shows the scatterplot between A_{DP} and K_{DP}. As before, scatter points are shown only for the equilibrium drop shape assumption. Unlike for A_h–K_{DP} relations discussed earlier, for A_{DP}–K_{DP} relations there is a very little dependence on the assumption of the drop shape factor b. The corresponding best-fit curves differ by not more than about 5% for b between 0.4 and 0.75 cm^{-1} and $K_{DP} > 0.25^{\circ}$ km^{-1}. This can be explained by the simultaneous and almost equal relative increase (decrease) of A_{DP} and K_{DP} as b increases (decreases) for a given DSD. The variability of A_{DP}–K_{DP} relations due to DSD details is higher than that for A_h–K_{DP} relations.

As can be seen from data scatter in Fig. 4 there is some slight nonlinearity in A_{DP}–K_{DP} relations. A nonlinear A_{DP}–K_{DP} relation, however, would result in a relatively cumbersome accounting for differential attenuation requiring nonlinear integrating estimates of K_{DP} along the radar beam. Given the fact that nonlinearity is not very significant and also because of relatively high variability due to DSD details (as compared with the variability of A_h–K_{DP} relations), it can be assumed that A_{DP} (dB km^{-1}) $\approx 0.032\ K_{DP}$ ($^{\circ}$ km^{-1}). In this case the total differential attenuation correction for Z_{DR} measurements can be given as

$$\Delta Z_{DR}\ (\mathrm{dB}) \approx a_2 \Phi_{DP}\ (^{\circ}). \tag{14}$$

Note that the coefficient obtained here ($a_2 = 0.032$ dB $^{\circ -1}$) is smaller than the one suggested by Bringi et al. (1990). Their estimate, based on gamma function DSD modeling for X band, yielded $a_2 = 0.045$ dB $^{\circ -1}$. Part of this difference, however, can be explained by the difference in considered wavelengths. Bringi et al. (1990) used $\lambda = 3$ cm, and here the NOAA X-band radar wavelength $\lambda = 3.2$ cm was used. The coefficients a_2 and a_1 decrease when the wavelength increases. Bringi et al. (1990) give $a_2 = 0.014$ dB $^{\circ -1}$ and $a_1 = 0.05$ dB $^{\circ -1}$ for $\lambda = 5.5$ cm.

These coefficients are also temperature dependent. A 5°C temperature increase from 5° to 10°C causes about a 4% increase in a_1 and about a 2.5% increase in a_2. It can be seen from Fig. 3 that the similar variability in a_1 can be caused either by a 5° temperature uncertainty or by an about 5% uncertainty in b. Ignoring the temperature dependencies of a_2 and a_1 can cause biases in attenuation-corrected radar reflectivities and differential reflectivities for large values of Φ_{DP}.

Since the combined polarimetric estimator (4) uses

TABLE 1. Dates, times, and accumulations (at the principal verification site) of rain cases observed during the Wallops experiment. Here A and B are the parameters of the case-tuned Z_e–R relations (for the horizontal polarization, i.e., $Z_e = Z_{eh}$; $Z_e = AR^B$).

Date	Duration	Accumulation (mm)	A	B
25 Feb 2001	1220–1520 UTC	7.3	276	1.49
4–5 Mar 2001	2100–0200 UTC	6.7	94	2.02
13 Mar 2001	0400–0630 UTC	2.7	234	1.63
13 Mar 2001	0930–1045 UTC	4.2	137	1.84
13 Mar 2001	1945–2045 UTC	1.8	203	1.57
15–16 Mar 2001	1700–0100 UTC	17.8	211	1.41
21 Mar 2001	0800–1730 UTC	42.4	624	1.34
30 Mar 2001	0330–0430 UTC	2.9	324	1.52
30 Mar 2001	0830–1200 UTC	8.4	334	1.32
1 Apr 2001	2100–2400 UTC	3.3	209	1.73
11 Apr 2001	0315–0615 UTC	8.9	221	1.75
11 Apr 2001	1430–1700 UTC	7.9	158	1.72
13 Apr 2001	1320–1600 UTC	4.6	216	1.87
16 Apr 2001	0000–0200 UTC	1.6	143	2.36
17 Apr 2001	0730–1000 UTC	5.0	227	1.79

power measurements, the process of calculating rainfall rate is iterative for each radar beam. At the first step, values of reflectivity and differential reflectivity corrected for attenuation $Z_e^{(1)}$ and $Z_{dr}^{(1)}$ are calculated from measured Z_e and Z_{dr} assuming the equilibrium drop shape [i.e., $b^{(0)} \approx 0.6$ cm^{-1}]. Values of $b^{(1)}$ are then recalculated using the corrected values of reflectivity and differential reflectivity in (3). If the difference between two consecutive estimates of b exceeds 10% (i.e., greater than the typical uncertainty of estimation of this parameter), the second correction reflectivity values are calculated and so on. At each step the estimate of rainfall rate is obtained using (4). The experience of using this method with real data indicates that just one iteration is needed for most practical situations.

3. Examples of X-band radar polarimetric measurements in rains of different intensity

During the two-month-long field campaign (21 Feb–19 Apr 2001), the NOAA ETL X-band radar was deployed at the National Aeronautics and Space Administration (NASA) Wallops Island facility. Prior to rain measurements, the radar was calibrated in an absolute sense using a corner reflector target. The polarimetric measurement scheme used for this experiment employed the transmission of a slanted 45° linear polarization with simultaneous receiving echoes on horizontal and vertical polarizations with two linear receivers. This scheme was proposed by Sachidananda and Zrnić (1985), and it is being considered for the polarimetric upgrade of the WSR-88D network radars (Doviak et al. 2000). Some research radars have already used this scheme (e.g., Scott et al. 2001; Holt et al. 1999).

The Wallops field project yielded 15 rain events with a total amount of precipitation for each event exceeding 0.1 in. as listed in Table 1. The principal verification site was located at a range of 3.3 km along the 134° azimuthal direction from the radar site. This site was equipped with two high-resolution (0.01 in.) rain gauges of the tipping-bucket type (one belonging to NOAA ETL and the other to NASA), and several disdrometers. Two other NOAA ETL high-resolution rain gauges were located along the 69° azimuthal direction at ranges of 6.6 and 14.7 km, respectively. The typical scan procedure included low-elevation sector scans with intermittent range–height indicator (RHI) scans.

Figure 5 shows four examples of radar measurements in rain of different intensities. All these examples correspond to one long event of 21 March 2001, when the rain gradually intensified from very light to very heavy. The radar beam in these examples is pointed in the direction of the gauge site (134° azimuth). The elevation angle (1.8°) was the lowest for which the ground clutter from Wallops Island structures could be neglected. The measured (total) differential phase shift (ϕ_{DP}) and reflectivity (Z_{eh}) scales for all the cases are the same for easier comparisons.

In a light rain (Fig. 5a), the trend of ϕ_{DP} is very small but still measurable. Typical standard deviation of ϕ_{DP} measurements due to noise was generally under 2°. The average K_{DP} value is only about 0.1° km^{-1}. Note that the corresponding K_{DP} value at S-band frequencies will be only about 0.03° km^{-1}, which may not reliably be measurable for reasonable range intervals. According to the ground-based gauge measurements at 3.3-km range, a rainfall rate near the time of this measurement (i.e., 1120:00 UTC) was about 2.4 mm h^{-1}. The radar reflectivity was less than about 30 dBZ for all the ranges within this beam. The attenuation correction for this example is small. At the 20-km range it is only about 1 dB.

Figure 5b shows an example of radar measurements when rainfall intensity increased a little in comparison with the time in Fig. 5a. According to the gauges at 3.3 km, the rainfall rate for this example was around 4 mm h^{-1} at the time of the measurements (1336:40 UTC). The ϕ_{DP} increase in the rain-filled area (up to about 20 km) is quite steady, though it is still quite small. The corresponding average K_{DP} value is about 0.25° km^{-1}. The maximum value of reflectivity correction is about 2 dB.

At 1430:40 UTC the rain became heavier (Fig. 5c). The 3.3-km rain gauge was indicating a rainfall rate of about 10 mm h^{-1} at the time of this measurement. The differential phase increase is very pronounced and steady as is the corrected value of the radar reflectivity of about 38 dBZ. The K_{DP} is about 0.8° km^{-1}. The low variability of K_{DP} indicates a rather uniform rain. At the longer ranges the attenuation correction for the reflectivity reaches about 10 dB. The steady values of the corrected reflectivity as a function of range in this uniform rain represent an independent qualitative check of the accounting for attenuation correction.

Figure 5d shows an example of measurements in very heavy rain. A cell with very high rainfall rates was observed near the radar at distances up to about 4 km. At

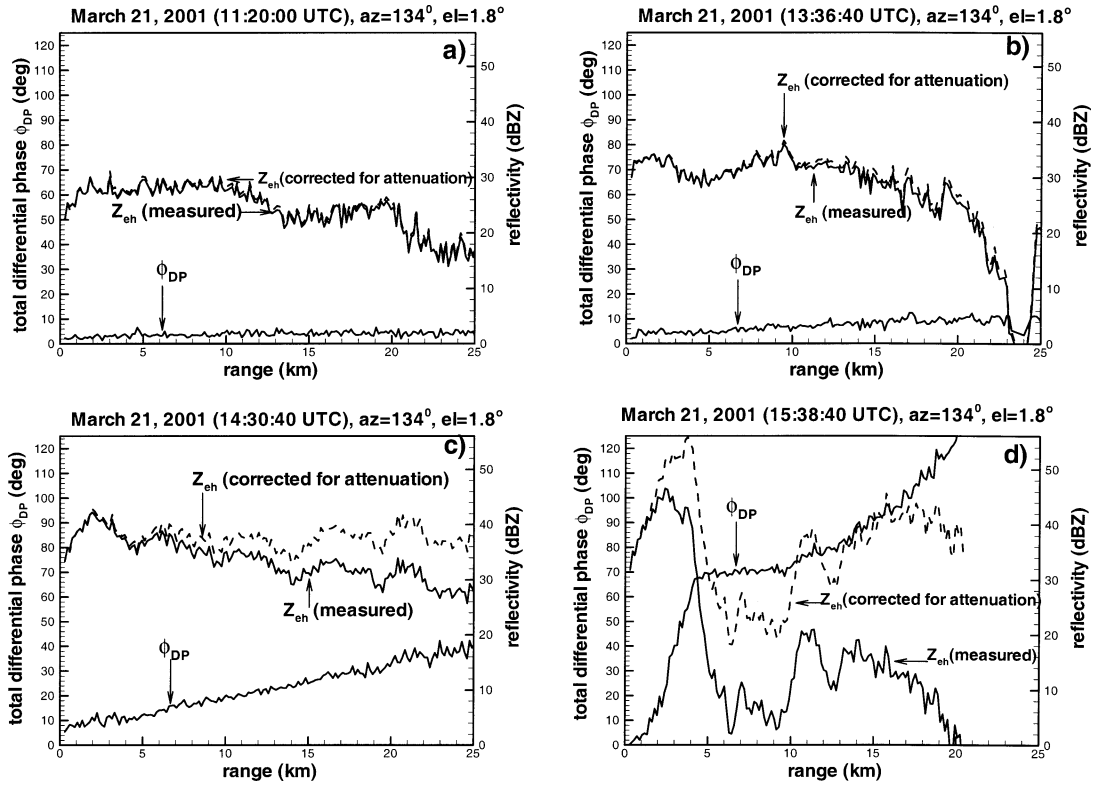

FIG. 5. Examples of radar polarimetric measurements in rains of different intensity: (a) very light rain, (b) light rain, (c) moderate rain, and (d) heavy rain. Solid and dashed reflectivity lines indicate measured values and those corrected for partial attenuation, respectively.

the time of these measurements, the high-resolution rain gauge was tipping once every 7 or 8 s, which corresponds to a rainfall rate of about 110–130 mm h^{-1}. There were no indications of hail in this cell. The measured differential phase shift ϕ_{DP} was increasing at a very high rate to about 4.5-km range with corresponding K_{DP} reaching up to 12–14° km^{-1}. Very light rain was observed between 5 and 10 km, followed by an area of moderate rain beyond 10 km. All these changes in rain are nicely seen in the Φ_{DP} pattern as a function of range. The attenuation in this heavy rain was significant. The received radar echoes decreased to the noise level beyond the range of about 20 km. The sensitivity of the radar at its current configuration is about 0 dB*Z* at 20-km range. For the Wallops experiment measurements, the transmitted power was about 4 dB down from its nominal value (about 16-kW peak power at each polarization) to avoid linear receiver saturations at very close ranges.

A remarkable fact about measurements in very heavy rains with X-band radar (such as in Fig. 5d) was the lack of the obvious manifestation of the backscatter phase shift δ that would appear as a ''bump'' on otherwise steady and monotonic changes of ϕ_{DP} (Hubert et al. 1993). It should be mentioned, however, that it is not the magnitude of δ that matters but rather the difference of backscatter phase shifts $\Delta\delta$ in the beginning and at the end of the interval used for estimation of K_{DP} as the range derivative of Φ_{DP} ($\Delta\phi_{DP} = \Delta\Phi_{DP} + \Delta\delta$, where $\Delta\Phi_{DP}$ is the differential phase shift on propagation).

Model calculations of the backscatter differential phase shift δ_i (for individual drops) are shown in Fig. 6 as a function of equal-volume drop diameter. At X band, δ_i is very small for $D_e < 3$ mm, but then it begins a monotonic increase at $D_e \approx 3$ mm. Since this increase is rather gradual, one could expect that $\Delta\delta$ will remain relatively small if the rainfall properties do not change very abruptly. The backscatter phase shift resonance at C band is more profound. It can be seen from Fig. 6 that if drops greater than about 5 mm are present, the backscatter phase shift at C band will be greater than at X band. It should be admitted that this is one possible explanation for the lack of significant backscatter differential phase shift effects in heavy rains observed at X band during the Wallops experiment. More heavy rain observations are needed to draw definitive conclusions about the wisdom of ignoring these effects. A filtering approach (e.g., Hubert and Bringi 1995) can be used to minimize effects of δ if they are significant.

4. Comparisons of radar-derived rainfall rates with gauge and disdrometer data

The combined polarimetric estimator (4), the equilibrium drop shape K_{DP}–R relation, and the mean and

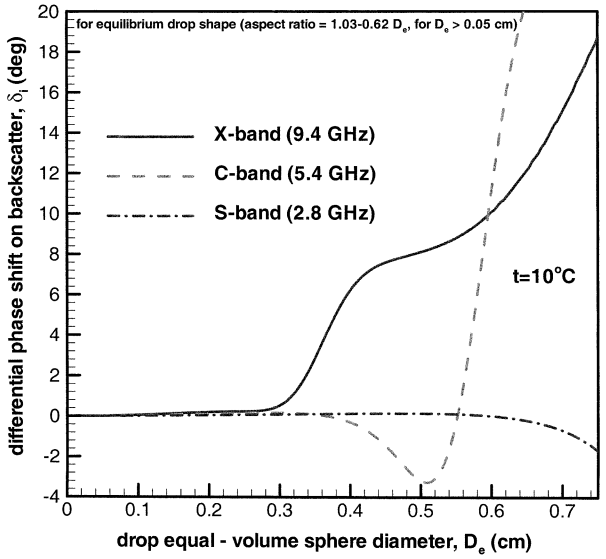

FIG. 6. The differential phase shift on backscatter as a function of equal-volume drop diameter.

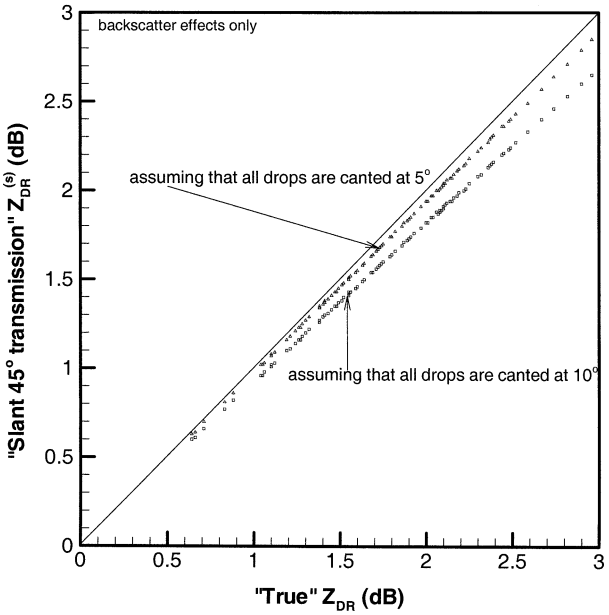

FIG. 7. Correspondence between differential reflectivities in the fast polarization switch mode (true Z_{DR}) and in the slant–45° transmission mode [$Z_{DR}^{(s)}$].

case-tuned Z_e–R relations were applied to the 15 rains observed during the Wallops experiment. The attenuation-corrected values of Z_{eh} were used in the Z_e–R relations. Specific differential phase shift on propagation, K_{DP}, was estimated as the range derivative of measured differential phase shift, ϕ_{DP}, using the least squares method applied for the sliding window range interval consisting of 25 range gates. The range gate resolution for the Wallops experiment was 150 m. The ϕ_{DP} measurements were filtered prior to estimating K_{DP}. The filtering procedure rejected all the data points that had low correlation between two consecutive pulses or were less than 3 dB above the noise floor of the radar (−103 dBm). Additional threshold applications, based on Doppler velocity measurements, rejected data points with suspected ground clutter contamination.

a. Differential reflectivity measurements used in the combined polarimetric estimator

As was mentioned above, the slant 45° transmission scheme with two receivers was used with the NOAA ETL X-band radar. Since the combined polarimetric estimator of rainfall rates (4) uses the differential reflectivity measurements, an estimation of how well the slant–45° scheme measurements of this parameter approximate classical differential reflectivity is necessary.

The slant–45° scheme offers some advantages such as the zero lag time between two copolar returns and a factor-of-2 increase of the number of samples for a given dwell. However, the differential reflectivity measurements, using this scheme, can be somewhat biased for canted drops through depolarization. It can be shown, however, that this bias is negligible for most practical cases. The true Z_{DR} and the slant 45° $Z_{DR}^{(s)}$ can be expressed as

$$Z_{DR} \approx \frac{\int \langle |S_{hh}(D_e)|^2 \rangle N(D_e)\, dD_e}{\int \langle |S_{vv}(D_e)|^2 \rangle N(D_e)\, dD_e} \tag{15}$$

$$Z_{DR}^{(s)} \approx \frac{\int \langle |S_{hh}(D_e) + S_{hv}(D_e)|^2 \rangle N(D_e)\, dD_e}{\int \langle |S_{vv}(D_e) + S_{vh}(D_e)|^2 \rangle N(D_e)\, dD_e}, \tag{16}$$

where S_{hh}, S_{vv}, S_{hv}, and S_{vh} are the elements of the amplitude backscatter matrix; the angular brackets denote averaging with respect to the canting angle α; and the integration carried out from 0 to $D_{max} \approx 6$ mm. For the zero cant, $Z_{DR} = Z_{DR}^{(s)}$ because nondiagonal elements S_{hv} and S_{vh} are proportional to $\sin(2\alpha)$. When drops are canted on average, $Z_{DR}^{(s)}$ differs from the true differential reflectivity. Since increasing (decreasing) of α from its mean value causes underestimation (overestimation) of Z_{DR} in the slant–45° transmission mode (though not exactly balanced), the mean canting angle is more important than its standard deviation, given that this standard deviation is relatively small.

Figure 7 shows the scatterplot between Z_{DR} and $Z_{DR}^{(s)}$ assuming that the drops are canted at 5° and 10° of vertical. Typical mean canting angles are of an order of this value or smaller. Calculations of differential reflectivities in Fig. 7 were performed for experimental DSDs

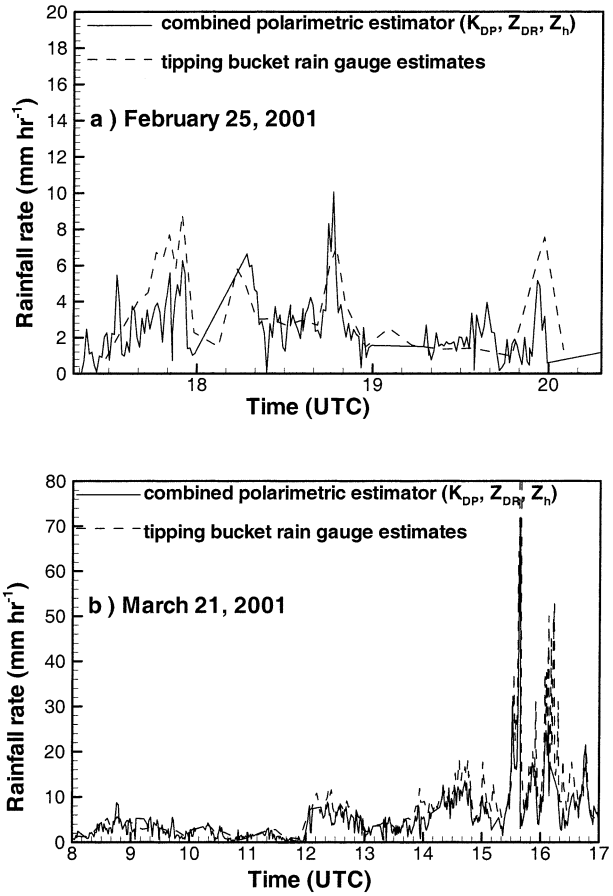

FIG. 8. Comparisons of rainfall rate estimates from the combined polarimetric estimator and from the high-resolution rain gauge for two rain events: (a) 25 Feb 2001 and (b) 21 Mar 2001.

and assuming the equilibrium drop shape model. It can be seen from this figure that the difference between Z_{DR} and $Z_{DR}^{(s)}$ does not usually exceed about 0.1 dB for a typical range of the variability of differential reflectivity in rains. Since this is less than the expected accuracy of Z_{DR} measurements, it is assumed when interpreting the experimental data in this study that $Z_{DR}^{(s)} \approx Z_{DR}$.

b. *Examples of comparisons of instantaneous rainfall rates*

Figure 8 shows examples of comparisons of instantaneous rainfall rate estimates from the radar measurements and from the data of ETL's high-resolution rain gauge located at the 3.3-km range in the 134° azimuthal direction from the radar site. Two representative cases from 15 rain events are shown. The combined polarimetric estimator (4) was used to derive radar estimates of rainfall rates, if radar reflectivity values corrected for attenuation exceeded 28 dB*Z*. For lighter rains, drops become rather spherical and the polarimetric signatures are not very pronounced. For these very light rains with $Z_e \leq 28$ dB*Z*, a mean Z_e–R relation was used to derive the rainfall rain estimates. The 3450 Wallops DSD spectra yielded the mean X-band relation for the entire experiment as $R = 0.038Z_e^{0.594}$ (i.e., $Z_e \approx 250R^{1.68}$), where Z_e here and hereinafter refers to the horizontal polarization reflectivity. The radar data correspond to the range gate centered above the gauge location. The radar resolution volume was approximately 150 m long and 50 m wide and was centered at about 100 m above the ground for this location. The time resolution of the radar estimates [the interval between two consecutive plan position indicator (PPI) sweeps] was about 45 s. The estimates from the rain gauge data in Fig. 8 correspond to mean rainfall rates between two consecutive tips (0.01 in.).

The comparisons for the long rainfall event of 21 March 2001 are shown in Fig. 8b. Note that examples of radar measurements along the beam for this event are also shown in Fig. 5. It can be seen that the agreement for the periods of light and moderate rain is rather close. Note that for the 9-h rain event of 21 March 2001, the reflectivity values above the gauge location were less than 28 dB*Z* for only two short periods just prior to 1100 and 1200 UTC, so more than 90% of rainfall rate estimates in Fig. 8b were obtained from the combined polarimetric estimator (4) and not from the mean Z_e–R relation.

During the heavier rain on 21 March 2001 after about 1530 UTC, the agreement between radar and gauges estimates of R is still generally close for values of R that are less than about 30 mm h^{-1}. However, the radar fails to catch the entire extent of rainfall rate peaks at around 1535 and 1610 UTC. At least part of the discrepancy may be attributed to the vast difference between radar and gauge sampling volumes.

Figure 8a shows rainfall estimate comparisons for the light-to-moderate rainfall event observed on 25 February 2001. The rainfall rates for this mostly stratiform event did not exceed about 10 mm h^{-1}, and there are practically no periods when the radar reflectivity above the gauge was less than 28 dB*Z*, so the radar estimates shown here are those from the combined X-band polarimetric estimator (4). As can be seen from Fig. 8a, the agreement of radar and gauge data is very close except for some difference between 1730 and 1800 UTC. The radar catches short-lived peaks of rainfall rates at 1845 and 1955 UTC.

c. *Comparisons of radar- and gauge-derived total accumulations*

Figure 9 shows the total accumulations of rainfall as a function of time for the two rain events discussed above. Results of different radar estimates are depicted in this figure. These include accumulations derived from the combined polarimetric estimator that uses K_{DP}, Z_{DR}, and Z_{eh} measurements; the equilibrium drop shape K_{DP}–R relation at X band ($R = 12.3K_{DP}^{0.81}$); the mean Wallops Z_e–R relation (i.e., $Z_{eh} \approx 250R^{1.68}$); and a case-tuned Z_e–R relation. The case-tuned Z_e–R relations were obtained for each of 15

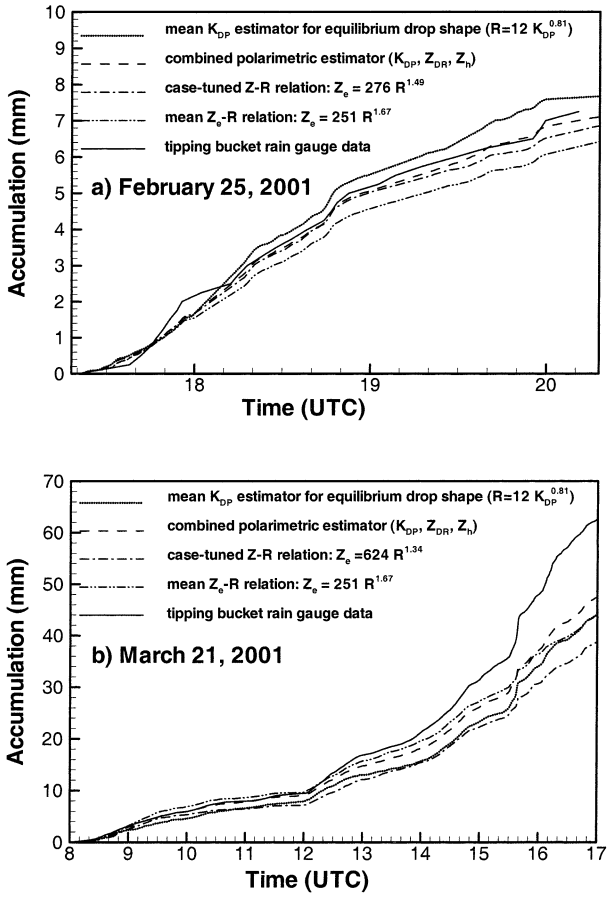

FIG. 9. Comparisons of rainfall accumulations from different radar estimators and from the high-resolution rain gauge for two rain events: (a) 25 Feb 2001 and (b) 21 Mar 2001.

rainfall events by considering DSDs measured by the disdrometer only during the particular event. The parameters for these case-tuned relations are given in Table 1, where it can be seen that the coefficient and the exponent varied widely from case to case. In addition to the radar estimates, data from the ETL high-resolution rain gauge are shown in Fig. 9. All the data in the figure correspond to the prime validation site mentioned above.

From different radar approaches, the combined polarimetric estimator gives the best agreement with the rain gauge. This agreement is not as good for the period of the very heavy rain (e.g., after 1530 UTC in Fig. 9b). For light and moderate rains combined, polarimetric estimates approximate gauge measurements rather closely. Comparisons as in Fig. 9 were performed for all 15 observational events recorded during the Wallops field experiment. Since there were three different validation sites equipped with ETL high-resolution rain gauges, it resulted in 45 data comparison points overall. During all the rain events used for comparisons, the radar reflectivity above the rain gauges did not exceed 28 dBZ for less than about 5% of total observational time, thus the combined polarimetric estimator (4) was used more than 95% of the time.

TABLE 2. Relative biases and standard deviations of rainfall accumulations obtained using different rainfall estimators (as compared with the tipping-bucket-type rain gauge data): the combined polarimetric estimator (4), the equilibrium drop shape K_{DP}–R relation ($R = 12.3K_{DP}^{0.81}$), the mean Z_e–R relation ($Z_{eh} = 250R^{1.68}$), and the case-tuned Z_e–R relations (reflectivity/differential reflectivity measurements were corrected for the attenuation/differential attenuation effects).

	Estimator			
	Z_{eh}, Z_{DR}, K_{DP}	K_{DP}–R	Mean Z_e–R	Case-tuned Z_e–R
Bias	−8%	−9%	−18%	−6%
Std dev	22%	30%	32%	23%

The mean relative bias and standard deviation (sd) between radar and gauge estimates of accumulation (A) were calculated for each radar estimator:

$$\text{bias} = \langle (A_r - A_g)A_g^{-1} \rangle, \tag{17}$$

$$(\text{sd})^2 = \langle (A_r - A_g)^2 A_g^{-2} \rangle, \tag{18}$$

where the angular brackets denote averaging, and subscripts r and g refer to the radar and gauge, respectively. Results of estimates using (17) and (18) are given in Table 2. Note that results obtained with all the estimators considered here were corrected for the altitude according to (5).

Assessments of bias and the standard deviation for the combined polarimetric estimator (K_{DP}, Z_{DR}, and Z_{eh}), the equilibrium drop shape K_{DP}–R relation at X band ($R = 12.3K_{DP}^{0.81}$), the mean Wallops Z_e–R relation (i.e., $Z_e \approx 250R^{1.68}$), and the case-tuned Z_e–R relations yield −8%, −9%, −18%, and −6% for bias, and 22%, 30%, 23%, and 32% for the standard deviation, respectively. Reflectivity values used in the Z_e–R relations were corrected for partial attenuation using differential phase shift measurements.

The combined polarimetric estimator gives the smallest overall standard deviation (22%), though the case-tuned Z_e–R relations provide almost the same value of the standard deviation (23%) with a slightly smaller bias. It should be noted, however, that the case-tuned Z_e–R relations generally are not known a priori and the polarimetric measurements at X band are still needed for accounting for attenuation in reflectivity measurements even if Z_e–R relations are used from the rainfall estimates. The use of the mean Z_e–R relation results in the most significant negative bias (−18%) and the largest standard deviation (32%). These bias and standard deviation data for different estimators are summarized in Table 2.

The equilibrium drop shape K_{DP}–R relation and the combined polarimetric estimator (4) provided similar biases for the total rainfall accumulation, although (4) was noticeably better in terms of the standard deviation. The similarity of biases is most likely due to the fact that the mean value of the shape factor b averaged over

all the recorded events was rather close to its equilibrium value for these rain events. The estimator (4) that intrinsically accounts for changes in the drop shape parameter b is superior to the equilibrium drop shape K_{DP}–R relation for estimates of instantaneous rainfall rates, and it is also expected to perform generally better for total accumulations for individual rain events when mean values of the shape parameter b are more likely to deviate from the equilibrium value compared to the average of many rain events. The case-tuned Z_e–R relations perform notably better than the mean relation, which provides the most significant bias and standard deviation.

One possible explanation of the small negative biases of both estimators that utilize differential phase shift measurements lies in the spread in drop canting angles, which was ignored when modeling K_{DP}–R relations in section 2a. This spread (σ_α) tends to reduce the coefficient in the K_{DP}–R relations by a factor of about $\exp(-2\sigma_\alpha^2)$ (Oguchi 1983). According to Ryzhkov (2001), a typical value of σ_α in rain is about 10°, which can amount to about 6% reduction of this coefficient. The small negative biases for the combined polarimetric estimator, the equilibrium drop shape K_{DP}–R relation, and the case-tuned Z_e–R relations are, however, close to the uncertainty of gauge measurements. An average difference in total accumulations measured by the collocated NASA and ETL rain gauges at one of the validation sites was about 10%.

5. Conclusions

One source of uncertainty in K_{DP}–R relations is due to variability in the raindrop oblateness–size dependence since the commonly assumed equilibrium drop shape is not unique. This dependence results in change of the coefficient in the K_{DP}–R relations while leaving the exponent almost intact. Tuning K_{DP}–R relations requires knowing b, the slope parameter of this dependence. A multiparameter scheme for estimating b, similar to the one suggested by Gorgucci et al. (2000) for S band, was derived here for X band. Modeling that led toward an approach to estimate b was done using the experimental raindrop size distributions rather than modeled ones.

As a result of modeling K_{DP}–R relations and the drop shape parameter b estimation algorithm, an X-band polarimetric estimator for instantaneous rainfall rates based on combined measurements of the specific propagation differential phase shift K_{DP}, differential reflectivity Z_{DR}, and the horizontal polarization reflectivity Z_{eh} was suggested. This estimator accounts for changes of the slope parameter b in the drop oblateness–size dependence and also for changes in drop fall velocities due to changes in the ambient air density.

Since the suggested polarimetric estimator uses power measurements (i.e., reflectivity and differential reflectivity), a procedure for correcting effects of the partial attenuation and differential attenuation based on measurements of differential phase shift was suggested. The differential phase capability thus offers a robust and relatively straightforward way of correcting for attenuation effects that traditionally have been a major obstacle to using X-band radar quantitative rainfall estimates based on power measurements.

The suggested X-band multiparameter polarization approach for rain measurements was tested with the transportable NOAA X-band radar that was recently upgraded in a polarimetric sense. The radar was deployed for an eight-week field experiment during February–April 2001 at the NASA Wallops Island base. Fifteen rain events were observed during this period. The ground validation equipment included three high-resolution tipping-bucket-type (0.01 in.) rain gauges deployed at three different locations and additional rain gauges and a Joss–Waldvogel disdrometer at one of these locations.

The observations included a wide range of rain conditions from very light rain with K_{DP} of about 0.1° km^{-1} to very heavy rain with K_{DP} reaching 12–14° km^{-1}. No significant effects of the backscatter phase shift were evident even in heavy rain, though more data are needed to better understand these effects. Comparisons of rainfall rate values estimated from gauges and obtained using the combined X-band polarimetric estimator proposed here were generally in good agreement for rainfall rates greater than about 1.5–2 mm h^{-1}. Lighter rains produce very subtle polarimetric signatures and the accuracy of polarimetric estimates degrades. Estimates of rainfall rates based on Z_e–R relations work better in these situations.

The quantitative comparisons of rainfall accumulations from different radar estimators and the high-resolution rain gauges were made for all 15 observed rain events. The mean Z_e–R relation (i.e., $Z_{eh} = 250R^{1.68}$) derived from 3450 DSD spectra recorded during the entire period of radar observations provided a mean relative bias of −18% and a mean relative standard deviation of 32% in comparison with the rain gauge measurements. Corresponding values of the bias and standard deviation for the case-tuned Z_e–R relations (i.e., derived from DSD spectra recorded only for the particular event) were −8% and 23%, respectively. However, case tuning of Z_e–R relations is not usually possible for real-time estimates.

The simplest polarimetric estimator based on the equilibrium drop shape K_{DP}–R relation at X band ($R = 12.3K_{DP}^{0.81}$) provided a −9% bias and a 30% standard deviation as compared with gauges. The best results in terms of agreement with the gauge data were obtained with the combined polarimetric estimator that uses measurements of K_{DP}, Z_{DR}, and Z_{eh} and tunes the value of the shape parameter b that describes the drop oblateness–size dependence. It yielded mean relative bias and standard deviation values of −8% and 22%, respectively. The similarity of mean biases for both polarimetric estimators is most likely due to the possible prox-

imity of the mean value of b for all the observed events to its equilibrium value. The combined polarimetric estimator is much superior to the equilibrium shape K_{DP}–R relation for estimations of instantaneous rainfall rates and total accumulations in individual events when the factor b deviates from its equilibrium value.

Both polarimetric estimators were used when values of reflectivity corrected for attenuation exceeded about 28 dBZ, which constituted more than 95% of total observation time above the gauges. Note that though the tuned Z_e–R relation and the combined polarimetric approaches provided similar results (in terms of bias and standard deviation), the latter approach should be considered superior since it does not use a priori information.

A small negative bias in the polarimetric and tuned Z_e–R relation estimates of rainfall accumulations may be explained by a number of factors, including canting angle spread and sampling issues. The magnitude of this bias is, however, of an order of uncertainty of gauge measurements themselves as determined by comparing data from two collocated tipping-bucket-type gauges.

Acknowledgments. The authors are thankful to C. W. Campbell, M. J. Post, L. I. Church, D. A. Hazen, J. S. Gibson, I. V. Djalalova, W. B. Madsen, and R. Rincon who participated in the Wallops experiment at different stages. This work was sponsored by NASA's Advanced Microwave Scanning Radiometer (AMSR) program and was facilitated by Dr. C. Kummerow.

REFERENCES

Andsager, K., K. V. Beard, and N. F. Laird, 1999: Laboratory measurements of axis ratios for large raindrops. *J. Atmos. Sci.,* **56,** 2673–2683.

Barber, P., and C. Yeh, 1975: Scattering of electromagnetic waves by arbitrarily shaped dielectric bodies. *Appl. Opt.,* **14,** 2864–2872.

Beard, K. V., 1985: Simple altitude adjustment to raindrop velocities for Doppler radar analysis. *J. Atmos. Oceanic Technol.,* **2,** 468–471.

Bohren, C. F., and D. R. Huffman, 1983: *Absorption and Scattering of Light by Small Particles.* John Wiley and Sons, 530 pp.

Brandes, E. A., A. V. Ryzhkov, and D. S. Zrnić, 2001: An evaluation of radar rainfall estimates from specific differential phase. *J. Atmos. Oceanic Technol.,* **18,** 363–374.

Bringi, V. N., V. Chandrasekar, N. Balakrishnan, and D. S. Zrnić, 1990: An examination of propagation effects on radar measurements at microwave frequencies. *J. Atmos. Oceanic Technol.,* **7,** 829–840.

Carey, L. D., S. A. Rutledge, D. A. Ahijevich, and T. D. Keenan, 2000: Correcting propagation effects in C-band polarimetric radar observations of tropical convection using differential propagation phase. *J. Appl. Meteor.*, **39,** 1405–1433.

Chandrasekar, V., V. N. Bringi, N. Balakrishnan, and D. S. Zrnić, 1990: Error structure of multiparameter radar and surface measurements of rainfall. Part III: Specific differential phase. *J. Atmos. Oceanic Technol.,* **7,** 621–629.

Doviak, R. J., V. Bringi, A. Ryzhkov, A. Zahrai, and D. Zrnić, 2000: Considerations for polarimetric upgrades to operational WSR-88D. *J. Atmos. Oceanic Technol.,* **17,** 257–278.

Gorgucci, E., G. Scarchilli, V. Chandrasekar, P. F. Meischner, and M. Hagen, 1998: Intercomparison of techniques to correct for attenuation of C-band weather radar signals. *J. Appl. Meteor.,* **37,** 845–853.

——, ——, ——, and V. N. Bringi, 2000: Measurement of mean raindrop shape from polarimetric radar observations. *J. Atmos. Sci.,* **57,** 3406–3413.

——, ——, ——, and ——, 2001: Rainfall estimation from polarimetric radar measurements: Composite algorithms immune to variability in raindrop shape–size relation. *J. Atmos. Oceanic Technol.,* **18,** 1773–1786.

Holt, A. R., V. N. Bringi, and D. Brunkow, 1999: A comparison between parameters obtained with the CSU-CHILL radar from simultaneous and switched transmission of vertical and horizontal polarization. Preprints, *29th Int. Conf. on Radar Meteorology*, Montreal, QC, Canada, Amer. Meteor. Soc., 214–217.

Hubert, J., and V. N. Bringi, 1995: An iterative filtering technique for the analysis of copolar differential phase and dual-frequency radar measurements. *J. Atmos. Oceanic Technol.,* **12,** 643–648.

——, V. Chandrasekar, V. N. Bringi, and P. Meischner, 1993: Processing and interpretation of coherent dual-polarized radar measurements. *J. Atmos. Oceanic Technol.,* **10,** 155–164.

Jameson, A. R., 1991: Polarization radar measurements in rain at 5 and 9 GHz. *J. Appl. Meteor.,* **30,** 1500–1513.

Keenan, T. D., D. Zrnić, L. Carey, P. May, and S. A. Rutledge, 1997: Sensitivity of C-band polarimetric variables to propagation and backscatter effects in rain. Preprints, *28th Int. Conf. on Radar Meteorology,* Austin, TX, Amer. Meteor. Soc., 13–14.

——, L. D. Carey, D. S. Zrnić, and P. T. May, 2001: Sensitivity of 5-cm wavelength polarimetric radar variables to raindrop axial ratio and drop size distribution. *J. Appl. Meteor.,* **40,** 526–545.

Kubesh, R. J., and K. V. Beard, 1993: Laboratory measurements of spontaneous oscillations for moderate-size raindrops. *J. Atmos. Sci.,* **50,** 1089–1098.

Martner, B. E., K. A. Clark, S. Y. Matrosov, W. C. Campbell, and J. S. Gibson, 2001: NOAA/ETL's polarization-upgraded X-band ''HYDRO'' radar. Preprints, *30th Int. Conf. on Radar Meteorology,* Munich, Germany, Amer. Meteor. Soc., 101–103.

Matrosov, S. Y., R. A. Kropfli, R. F. Reinking, and B. E. Martner, 1999: Prospects for measuring rainfall using propagation differential phase in X- and K_a-radar bands. *J. Appl. Meteor.*, **38,** 766–776.

——, ——, K. A. Clark, and W. C. Campbell, 2001: Multi-parameter polarimetric estimators of rainfall rate at X-band. Preprints, *30th Int. Conf. on Radar Meteorology,* Munich, Germany, Amer. Meteor. Soc., 609–611.

May, P. T., T. D. Keenan, D. S. Zrnić, L. D. Carey, and S. A. Rutledge, 1999: Polarimetric radar measurements of tropical rain at a 5-cm wavelength. *J. Appl. Meteor.*, **38,** 750–765.

Oguchi, T., 1983: Electromagnetic wave propagation and scattering in rain and other hydrometeors. *Proc. IEEE,* **71,** 1029–1078.

Pruppacher, H. R., and R. L. Pitter, 1971: A semi-empirical determination of the shape of cloud and rain drops. *J. Atmos. Sci.,* **28,** 86–94.

——, and J. D. Klett, 1978: *Microphysics of Clouds and Precipitation.* D. Reidel, 714 pp.

Ryzhkov, A. V., 2001: Interpretation of polarimetric radar covariance matrix for meteorological scatterers: Theoretical analysis. *J. Atmos. Oceanic Technol.,* **18,** 315–328.

——, and D. S. Zrnić, 1995: Comparisons of dual-polarization radar estimators of rain. *J. Atmos. Oceanic Technol.,* **12,** 249–256.

Sachidananda, M., and D. S. Zrnić, 1985: Differential propagation phase shift and rainfall estimation. *Radio Sci.,* **20,** 907–922.

Scott, R. D., P. R. Krehbiel, and W. Rison, 2001: The use of simultaneous horizontal and vertical transmissions for dual-polarization radar meteorological observations. *J. Atmos. Oceanic Technol.,* **18,** 629–648.

Testud, J., E. L. Bouar, E. Obligis, and M. Ali-Mehenni, 2000: The rain profiling algorithm applied to polarimetric weather radar. *J. Atmos. Oceanic Technol.,* **17,** 332–356.

Zrnić, D. S., and A. Ryzhkov, 1996: Advantages of rain measurements using specific differential phase. *J. Atmos. Oceanic Technol.,* **13,** 454–464.

——, T. D. Keenan, L. D. Carey, and P. May, 2000: Sensitivity analysis of polarimetric variables at a 5-cm wavelength in rain. *J. Appl. Meteor.,* **39,** 1514–1526.